Journal of Asian Ceramic Societies 2 (2014) 44–51

Contents lists available at ScienceDirect

Journal of Asian Ceramic Societies

journal homepage: www.elsevier.com/locate/jascer

# Animal trial on zinc doped hydroxyapatite: A case study

Promita Bhattacharjee[a], Howa Begam[a,*], Abhijit Chanda[a], Samit Kumar Nandi[b]

[a] School of Bioscience & Engineering, Jadavpur University, Kolkata 700032, India
[b] West Bengal University of Animal and Fishery Sciences, Kolkata, India

ARTICLE INFO

*Article history:*
Received 2 October 2013
Received in revised form 7 January 2014
Accepted 7 January 2014
Available online 4 February 2014

*Keywords:*
Calcium hydroxyapatite
Histopathology
Radiology
Bioresorption
Oxytetracycline

ABSTRACT

Calcium hydroxyapatite (HAp) has widely been used as bone substitute due to its good biocompatibility and bioactivity. In the present work, hydroxyapatite was doped with zinc (Zn) to improve its bioactivity. The study reports the technique to synthesize Zn-doped HAp powder using a simple, economic route and the influence of this dopant on the physical, mechanical and biological properties of the HAp. Porous blocks were prepared by sintering at 1150 °C and the sintered samples were characterized using XRD and FTIR. In vitro bioresorption behavior of the sintered blocks was assessed in simulated body fluid (SBF) maintained in a dynamic state. The in vivo study was exclusively conducted to evaluate healing of surgically created defects on the tibia of adult New Zealand rabbit after implantation of HAp. Local inflammatory reaction and healing of wound, radiological investigations, histological and SEM studies, oxytetracycline labeling and mechanical push-out test were performed up to 60 days post-operatively. It was observed that Zn substituted HAp showed better osteointegration than undoped HAp. Radiology revealed progressively less contrast between implant and surrounding bone. New bone formation in Zn-doped HAp was more prompt. Mechanical push-out test showed high interfacial strength (nearly 2.5 times) between host bone and doped implant.



## 1. Introduction

The hard tissue of human bone consists of inorganic calcium phosphate, organic collagen and water. In cortical (compact) bone, calcium hydroxyapatite [$Ca_{10}(PO_4)_6(OH)_2$; HAp] crystals are found within collagen as needles oriented in the direction of the fibers [1–3]. In the last few decades synthetic bone grafts in the form of calcium HAp has been developed following various techniques. It has achieved significant applications in wide variety of orthopedic and dental applications. But it has its own limitations; it is inherently brittle and it is not osteoinductive, but only osteoconductive in nature. Researchers are still working to find suitable means to improve the mechanical and biological properties of HAp. One approach is to make a composition, which is similar to that of phosphatic material available in human bone.

Bone mineral contains several ionic substitutions like sodium (Na), zinc (Zn), magnesium (Mg), iron (Fe) and carbonate ($CO_3^{2-}$). These substitutions induce complex structures at the unit cell level and play a role in influencing the dissolution rate of apatites, which may favor osseointegration [4]. These foreign ions also control the crystallinity, lattice structure and microstructure of the HAp. Among these ions, Zn ions have drawn considerable attention of the research groups due to their inhibitory activity to osteoclastic bone resorption. Bigi et al. [5] investigated the role of Zn on crystal growth and thermal stability of HAp. They showed that the presence of Zn in solution strongly inhibits the crystallization of hydroxyapatite. Webstar et al. [6] reported that Zn had a typical role in promoting new bone formation. It found to inhibit osteoclastic bone resorption and induces apoptosis of mature osteoclasts. Bandyopadhyay et al. [7] reported that Zn addition increases densification and mechanical properties like hardness of HAp. Ito et al. observed that doping with Zn in amounts between 0.6 and 1.2 wt% enhanced the proliferation of mouse osteoblast-like cells in a tricalcium phosphate/HAp composite ceramic [8]. Wang et al. [9] developed Zn-containing HAp layers on the Ti rods which showed more effective increases in fibroblast proliferation.

Most of these works addressed the effect of doping on the enhancement of mechanical, physical properties and reported in vitro cell culture results. Only a few [10–12] animal trial reports on doped HAp are available till date. They focused on only one

* Corresponding author. Tel.: +91 9477081528.
*E-mail address:* howabegam@gmail.com (H. Begam).

Peer review under responsibility of The Ceramic Society of Japan and the Korean Ceramic Society.

Production and hosting by Elsevier

2187-0764 © 2014 The Ceramic Society of Japan and the Korean Ceramic Society. Production and hosting by Elsevier B.V. All rights reserved.
http://dx.doi.org/10.1016/j.jascer.2014.01.005

or two methods to assess the extent of bone remodeling. In the present work, we have developed Zn-doped porous HAp scaffolds through a wet chemical method and studied their detailed in vivo performance in critical sized tibial defects of rabbits. Undoped HAp was used as the control to make a comparative analysis. Detailed animal trial involved radiology, scanning electron microscopy, histopathology and oxytetracycline study. Finally the mechanical push-out tests were carried out to assess the strength of the bone–implant interface.

## 2. Materials and methods

### 2.1. Fabrication of scaffolds

HAp powder was prepared using wet chemical method by drop wise addition of ortho-phosphoric acid ($H_3PO_4$) to a starting solution of calcium hydroxide ($Ca(OH)_2$). The solution was continuously stirred at 80 °C with pH of 11–12. For Zn-doped HAp, measured quantities of ZnO were incorporated into the $Ca(OH)_2$ suspension before the addition of $H_3(PO)_4$ solution. The solution was filtered and washed thoroughly with distilled water after 24 h. After overnight drying at 90 °C, the HAp powder was crushed and sieved. The as prepared powder was calcined at 800 °C for 2 h in air atmosphere in an electric resistance furnace. The calcined HAp powders were pressed at a pressure of 150 MPa in a uniaxial press (PEECO Hydraulic Pvt Ltd., capacity 20 ton) to form the pellets with radius $12.5 \pm 0.05$ mm and thickness $5.4 \pm 0.05$ mm. The pellets were sintered at 1150 °C with soaking time of 2 h and heating rate 3°/min in air atmosphere.

### 2.2. Characterization of powder and sintered blocks

Material phase and lattice parameters of the HAp powders and sintered blocks were evaluated using XRD (Model-Miniflex, Rigaku Co., Tokyo, Japan). Crystallinity ($X_c$) of the samples was determined with the following expression: $X_C = 1 - (V_{112/300}/I_{300})$, where, $V_{112/300}$ is intensity of hollow between the planes (1 1 2) and (3 0 0) reflections and $I_{300}$ is the intensity of (3 0 0) reflection [13]. Lattice parameters ($a$ and $c$) were calculated from peaks (3 0 0) and (0 0 2), respectively, using the standard HCP unit cell plane spacing relationship [14]. The volume ($V$) of the hexagonal unit cell of each HAp formulation was calculated using standard crystallographic equation [15].

FTIR analysis was also made in mid IR region (4000–400 $cm^{-1}$) using KBr pellets in a Perkin-Elmer (Model 1615, USA) instrument. The micro-structural features of the fractured surfaces were obtained by scanning electron microscopy (SEM; S3000N, Hitachi, Japan). EDX analysis was performed to check the presence of elements in the fractured samples (JEOL; JSM-6360, Japan).

### 2.3. In vitro study

The rate of bioresorption of sintered undoped and doped HAp structures was determined in terms of their weight loss or gain as a function of time, in a protein-free dynamic simulated body fluid (SBF). Specimens of undoped HAp and doped HAp were immersed in a freshly prepared SBF under static condition in an incubator at 37 °C for 4 weeks. Over the whole course of the study, the SBF was changed once in every 3 days. Surface microstructures of these samples were observed using SEM to study the extent of mineralization at the top layer.

### 2.4. In vivo study

Animal experimentation was carried out following the procedures conforming to the standards of the Institutions' Animal Ethical Committee of the West Bengal University of Animal and Fishery Sciences, Kolkata, India. A total of eight healthy New Zealand white rabbits of either sex, weighing 2–2.5 kg were randomly distributed into two groups: control group I (4 animals in which pure HAp implants were inserted within the created defects) and the test animals, group II (4 animals in which Zn-doped HAp ceramics were inserted within the created defects). Fig. 1 showed the well placed HAp scaffold in rabbit tibia. The specimen was implanted along the longitudinal direction in the rabbit tibia.

Surgery was performed under aseptic conditions and sedation by injection of Xylazine hydrochloride (XYLAXIN®, Indian Immunologicals, India) at a dose of 1 mg/kg body weight and Ketamine hydrochloride (Ketalar®, Parke-Davis, India) at a dose of 25 mg/kg body weight intramuscularly. A bone defect (5 mm × 2.5 mm × 3 mm) in all the animals was created in the medial aspect of proximal tibia bone with the help of a motorized dental drill. In all the animals, implants were secured in position by suturing muscle, subcutaneous tissue and skin in layers. All the treated animals were administered using injection, Cefotaxime sodium (Mapra India, India) at a dose rate 125 mg/kg of body weight intramuscularly, at 12 h interval daily for 5 days and Meloxicam (MELONEX®, Intas Pharmaceuticals, India) at 0.2 ml once daily for 5 days. Surgical wounds were dressed daily with Povidone iodine and antibiotic ointment for 10 days post-operatively.

Radiographs were taken immediately after implantation and subsequently on days 15, 30, 45 and 60 post-operatively of the operated proximal tibia for studying the status of implant and host bone reaction to implant.

New bone formation on and surrounding the implant was verified by detailed SEM study (Jeol JSM 5200 model) at the end of study of 60 days. After removing the soft tissue, the implanted bone specimens were fixed in 5% glutaraldehyde phosphate solution, washed twice for 30 min with phosphate-buffered saline (pH 7.4) and distilled water and then dehydrated in a series of graded alcohol solutions. Finally samples were dried with hexamethyldisilizane. A gold conductive coating was applied by ion sputtering (JEOL ion sputter, model JFC 1100, Japan) at 7–10 mA and 1–2 kV for 5 min. The resin-mounted sample surfaces were then examined under SEM after proper alignment to understand the orientation and distribution of newly formed osseous tissues and distribution/absorption of materials at the defect site.

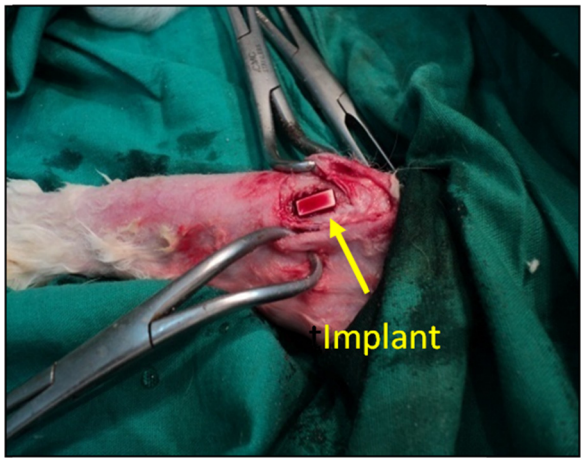


**Fig. 1.** Implant inserted within the defects.

The proximal tibias were harvested for histological analysis to check the cellular response of host bone to the implants. Bone specimens from adjacent bone at the side and at the bottom of the original bone defect were collected and washed thoroughly with normal saline and were fixed in 10% formalin for 7 days. All specimens of bone tissue were decalcified (Goodling and Stewart's fluid containing formic acid 15 mL, formalin 5 mL and distilled water 80 mL solution), followed by fixation with 4% paraformaldehyde. The samples were then embedded into paraffin wax, 4 μm sections were prepared and stained with hematoxylin and eosin.

Fluorochrome (oxytetracycline dehydrate; Pfizer India, India), at a dose of 25 mg/kg body weight, was given 3 weeks before sacrificing the animals, i.e., on 35, 36, 43, and 44 days (2-6-2 manner) post-operatively for double-toning of new bone. Undecalcified ground sections were prepared from the implanted segments of bone and the sections were ground to 20 μm thickness using different grades of sand paper. The ground undecalcified sections were observed under ultraviolet incidental light with an Orthoplan microscope (Excitation filter, BP-400 range, Leitz, USA) to analyze bone formation within the implants.

Mechanical push-out test was carried out at 60 days post-operatively to check the interfacial strength of the host bone to the implant. After removal of soft tissue, the implanted proximal tibia bones of two groups were refrigerated in gauze dampened with physiological saline. The proximal and distal radial metaphyses were excised, leaving the proximal diaphyseal segment containing the implants. Each implant was pushed out of the tibia bone with a plunger of rectangular cross-section. The samples were placed on a support jig, with a hole larger in diameter than the implant perimeter. For the push-out test, a universal testing machine (Instron 5500R, UK) was used at a constant crosshead speed of 0.5 mm/min.

## 3. Results and discussion

### 3.1. Characterization of calcined powder

The XRD pattern of pure and doped HAp calcined at 800 °C was shown in Fig. 2. Both pure and doped HAp showed characteristic peaks of HAp at $2\theta = 31.7°$ (2 1 1), 32.9° (3 0 0), 25.88° (0 0 2) which matched well with JCPDS pdf no. 09-0432. Another peak was observed in case of doped HAp at $2\theta = 11.5°$ which was matched with zinc phosphate hydrate ($Zn_3(PO_4)_2 \cdot xH_2O$) (JCPDS pdf no. 09-0125). Crystallinity of pure HAp was 75% whereas the crystallinity for the doped HAp was marginally lower.

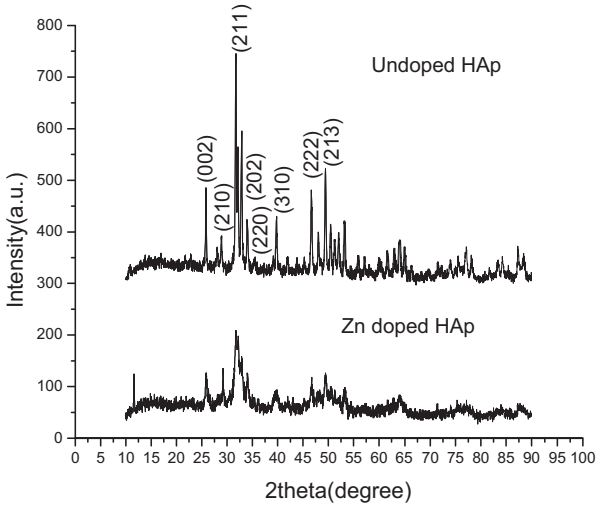


**Fig. 2.** XRD pattern of pure and doped HAp powder calcined at 800 °C.

**Table 1**
Lattice parameter of pure and doped HAp powder.

| Sample | *a* axis (Å) | *c* axis (Å) | Unit cell volume (Å$^3$) |
|---|---|---|---|
| Pure HAp | 9.4224 | 6.8980 | 1580.03 |
| Doped HAp | 9.4352 | 6.8772 | 1579.55 |

The lattice parameter of the pure and doped HAp is given in Table 1. The ionic radius of Zn (0.074 nm) is less than Ca (0.099 nm). The difference in ion size was reflected in the variation of lattice parameters. Doped HAp showed reduction in the *c* axis and also in unit cell volume. But the *a* axis was found to increase in case of doped HAp. Such a variation can be explained in the light of explanation given by Miyaji et al. [16]. As per their proposition the presence of lattice $H_2O$ which substitutes $OH^-$ in HAp was responsible for the simultaneous increase in *a* axis and decrease in *c* axis.

Fig. 3 shows the FTIR spectra of calcined pure and doped HAp. A bulge peak at 3453 $cm^{-1}$ is observed for the doped HAp which reveals $OH^-$ group. The broad $OH^-$ peak of the doped HAp signifies effect of Zn dopant and more amount of lattice $H_2O$. In case of pure HAp this $OH^-$ group peak at 3575 $cm^{-1}$ was very short and tending to disappear. The peak for $CO_3^{2-}$ was found at 1415 $cm^{-1}$ for the both powders. The presence of $PO_4^{3-}$ group was observed at 610 $cm^{-1}$, 558 $cm^{-1}$ and 637 $cm^{-1}$. In the doped HAp, the $PO_4^{3-}$ group was present at 1030, 596 and 558 $cm^{-1}$. No peak for TCP was observed.

### 3.2. Characterization of sintered HAp

The bulk density of the green and sintered specimens was calculated using gravimetric method by measuring the volume and mass. Fig. 4 shows the sintered as well as green density. The green density of both specimens was found to 1.66 g/cm$^3$.

Bulk density after sintering in both the cases was closely similar. In undoped HAp sintered density was 2.98 g/cm$^3$ and for doped HAp density was 2.85 g/cm$^3$. As such there was no prominent effect of dopant on densification.

The sintered specimens were also studied with XRD to assess the effect of heating on the formation of various phases. X-ray powder diffraction analysis of the sintered undoped and Zn-doped HAp structures are presented in Fig. 5. The major peak was observed at 31.77° (2 1 1) for pure HAp and it was phase pure. In Zn-doped HAp for (3 0 0) plane peak was observed at $2\theta = 32.9°$ and other two peaks got slightly shifted (31.5° for (2 1 1) plane and 26.1° for (0 0 2) plane). In this context it may be noted that with

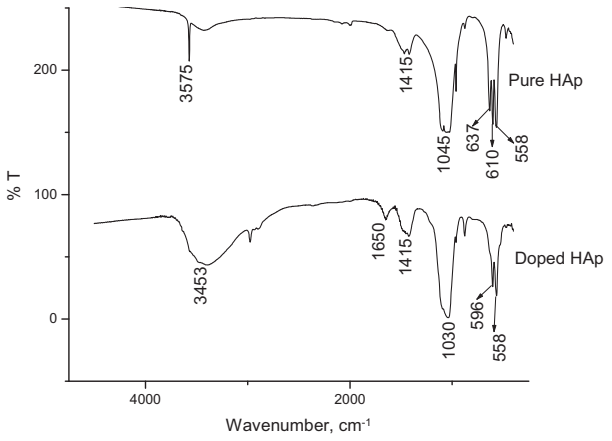


**Fig. 3.** FTIR pattern of pure and doped HAp powder calcined at 800 °C.

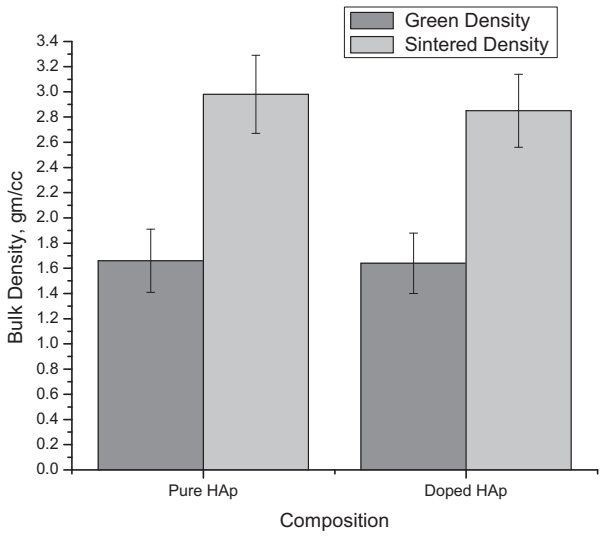


**Fig. 4.** Bulk density of pure HAp and doped HAp sintered at 1150 °C.

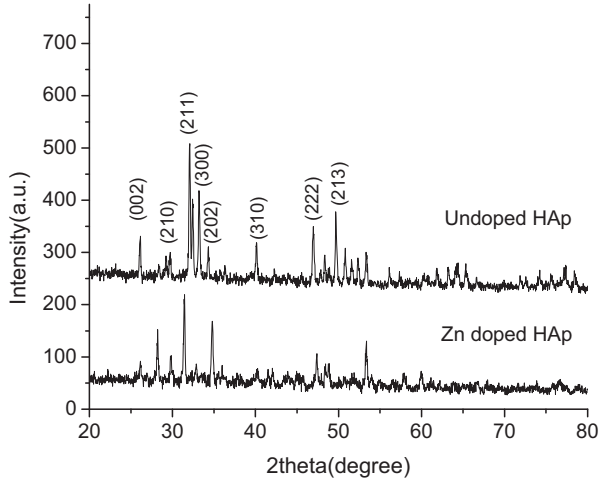


**Fig. 5.** XRD pattern of pure and doped HAp sintered at 1150 °C.

introduction of Zn, variation in crystal structure (*c* and *a* axes) took place and the slight shift in XRD can be attributed to this. The Zn-doped HAp consisted of some amount of β-TCP as well at $2\theta = 34.4^\circ$ (2 2 0) which matched with JCPDS pdf no. 09-0169. The crystallinity of pure HAp was 51% and a closely similar (49%) crystallinity was observed for the Zn-doped HAp.

Table 2 shows the lattice parameters for the sintered components. From the above table it was observed that *a* axis of the doped HAp was reduced. This was contradictory to the results obtained in case of calcined powders. In the absence of lattice $H_2O$ (evaporated during sintering), the Zn ion with lower ionic radius size replaced the Ca ion from the HAp structure and caused reduction of *a* axis. At the same time *c* axis increased in length. This increase in *c* axis due to doping may be attributed to the interstitial mechanism of Zn insertion into HAp unit cell, as proposed by Gomes et al. [17].

**Table 2**
Lattice parameter of sintered pure and doped HAp.

| Sample | *a* axis (Å) | *c* axis (Å) | Unit cell volume (Å$^3$) |
|---|---|---|---|
| Pure HAp | 9.434 | 6.8983 | 1589.52 |
| Doped HAp | 9.4205 | 6.9096 | 1587.57 |

Insertion of a small Zn cation created linear O—Zn—O units oriented along the *c* hexagonal axis and increased *c* axis of the unit cell [17].

Fig. 6a and b shows the microstructure of pure and doped HAp respectively sintered at 1150 °C. The grains were uniform and round shaped. The average grain size of the pure HAp was $0.9 \pm 0.13$ μm and for doped HAp it was $1.27 \pm 0.19$ μm. Interconnected pores were observed in both. This interconnectivity of pores was expected to play an important role in promoting tissue growth during in vivo tests. Fig. 6c shows the EDX analysis of Zn-doped HAp. In undoped HAp, Ca:P ratio was 1.66. Here we calculated (Ca + Zn):P ratio from the EDX data. It was around 1.67 which is similar to the ideal stoichiometric Ca:P ratio in HAp.

### 3.3. Biological characterization

#### 3.3.1. In vitro study

From the bioresorption analysis, it was observed that there was no significant weight loss for undoped and doped HAp. Rather weight of both types of specimen increased, by 0.54% for undoped HAp and 0.97% for doped HAp. Such a weight gain indicated the formation of new material (HAp layer on the surface). SEM micrographs as shown in Fig. 7 revealed the formation of HAp on the surface of both undoped and doped HAp (Fig. 7a and b). We carefully scrapped off the layer from the sample surface. Fig. 7c shows EDX of that scrapped layer on the surface of Zn-doped HAp. It showed that even after SBF exposure for 28 days, predominantly Ca and P (but not Zn) were found. Ca:P ratio was similar to that of HAp. It was observed that the apatite formed throughout the surface area in both cases and formed a clustered, multilayered flower like structure. Fig. 7d shows the XRD of that scrapped layer which shows peaks at $2\theta = 31.7^\circ$ (2 1 1), 32.19° (1 1 2), 32.9° (3 0 0), 25.8° (0 0 2) which matched nicely with the standard XRD peaks of HAp.

#### 3.3.2. In vivo study

*3.3.2.1. Local inflammatory reactions and healing of wound.* No marked inflammatory reactions were observed in both the control and the experimental group following placement of bio-ceramic implant up to 60 days post-operatively. No foreign body response or toxicity was elicited and hence it was confirmed that the implant was accepted as a suitable alternative bone graft to fill the defect.

#### 3.3.3. Radiological observations

Critical evaluation of radiographs taken at different intervals in animals of group II revealed appreciable evidence of fracture union as compared to group I (control group) as shown in Fig. 8. However, at the initial stages, minimal periosteal reaction and smoothen of edges of cortical bone defects were noticed. The radiograph revealed clearly that progressively the difference in radio density between doped implant specimen and surrounding host bone tissue diminished (Fig. 8Ia and Ie). Subsequently, there was substantial reduction of gap size by newly formed osseous tissue, making the defect more round and smooth (Fig. 8IIe). It was indicative of better tissue-implant interaction with time.

#### 3.3.4. Histological studies

Fig. 9 shows hematoxylin and eosin (HE) staining images of samples after 2 months, post-surgery, exhibiting the cellular responses between the implants and the host bone tissues. Group-I as shown in Fig. 9a (pure HAp) section showed no marked inflammatory reaction with moderate fibro-collagenization and normal architecture of bony lamellae along with development of Haversian system. Well defined periostium and Volkmann's canal were observed. The lacunae in some places showed fibro-ostic proliferation of bony stroma indicating normal histogenesis of bone. Group II in (Zn-doped HAp) section showed well-formed vascular sinuses along

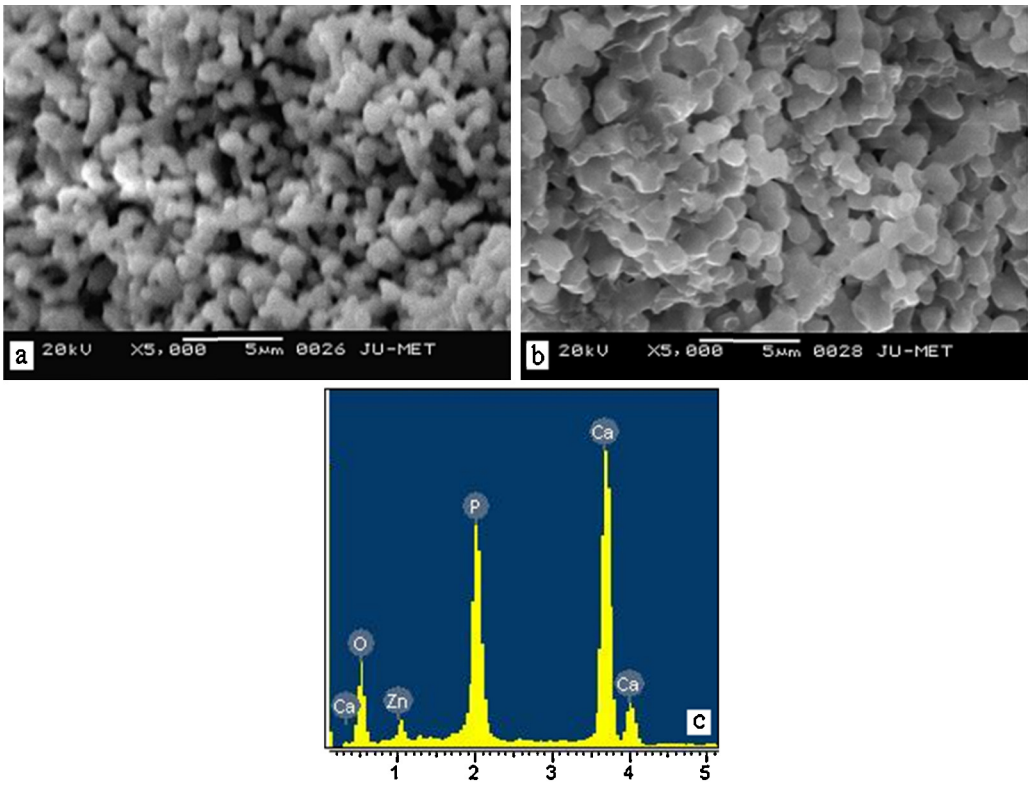


**Fig. 6.** SEM micrograph of (a) pure HAp and (b) doped HAp. (c) EDX pattern of doped HAp.

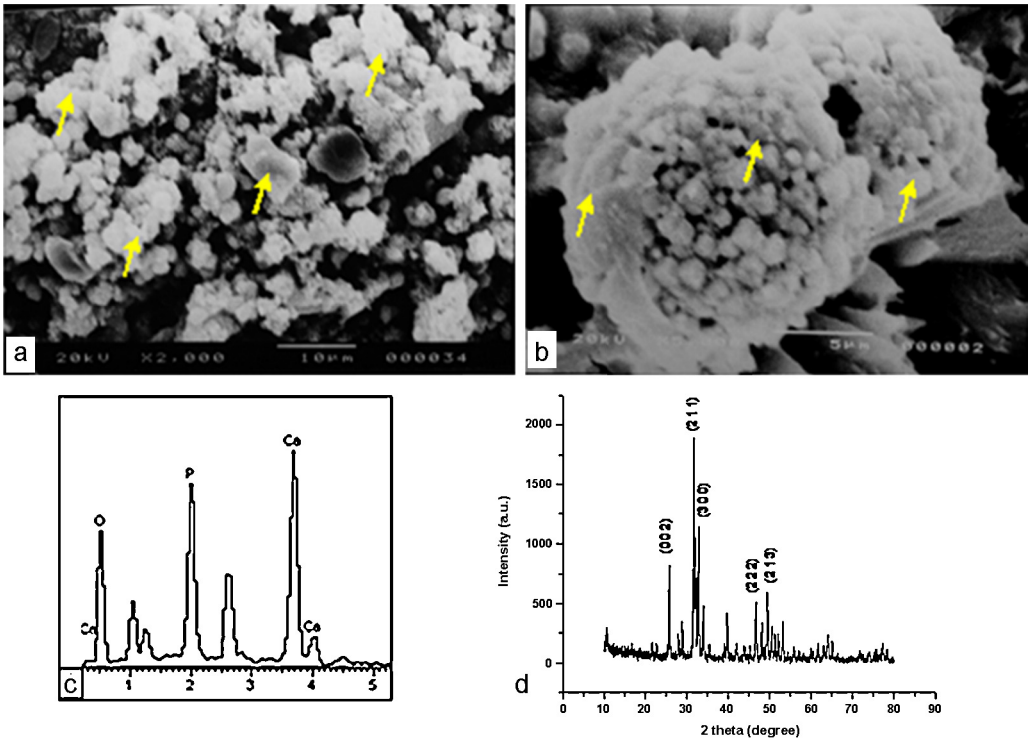


**Fig. 7.** SEM micrograph of apatite formation (shown by arrows) on surface of (a) undoped and (b) doped HAp ceramics received after 4 weeks in simulated body fluid (SBF). (c) EDX and (d) XRD patterns of apatite layer in case of Zn-doped HAp.

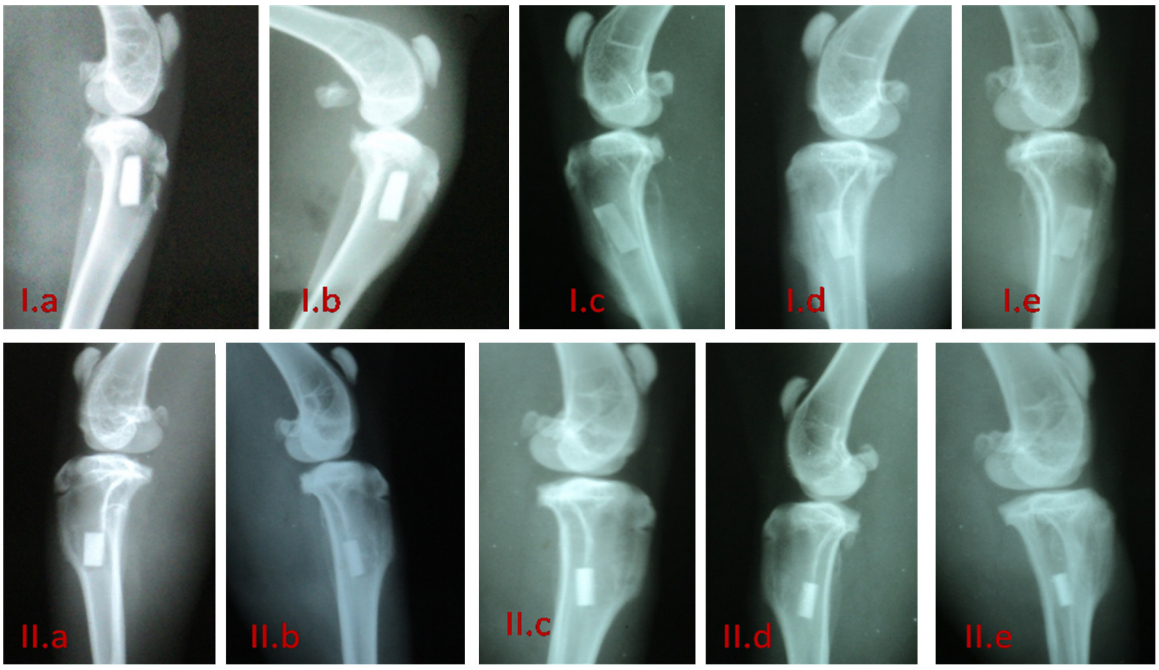


**Fig. 8.** Serial radiographs at different days of interval post-operatively of I – pure HAp and II – doped HAp (a – 0th day, b – 15th day, c – 30th day, d – 45th day, e – 60th day).

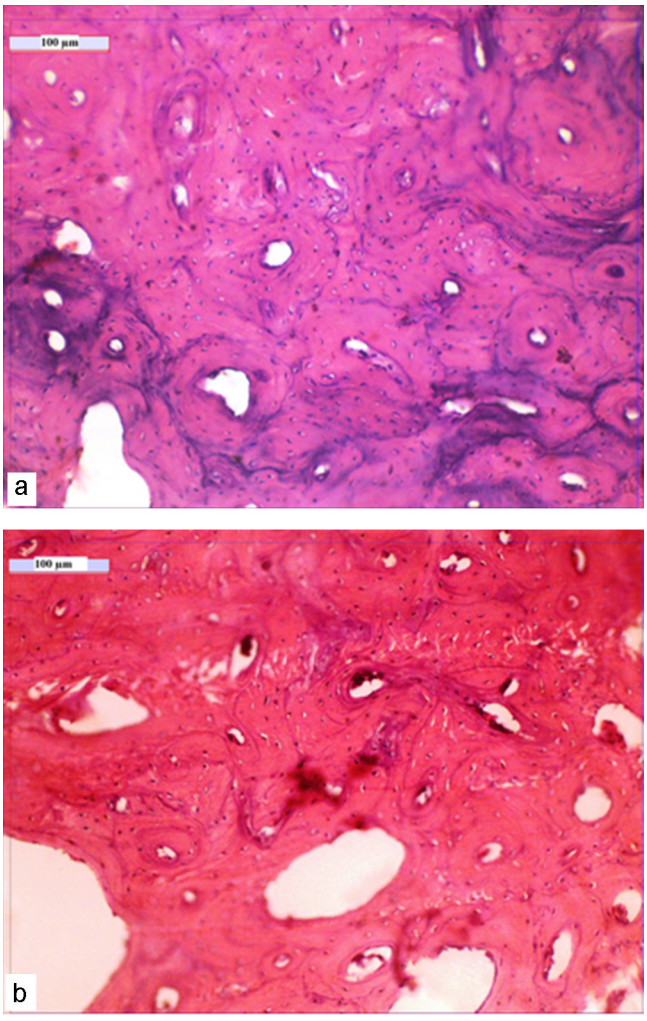


**Fig. 9.** Hematoxylin and eosin (HE) staining histological images at 2 months post-operatively (a, Haversian system and b, bony lamella).

with osseous stroma mainly Haversian canal, canaliculi and intermingling sinusoidal spaces (lacunar spaces) as shown in Fig. 9b. The bony tissues showed well-arranged mineralization along with supporting cellular infiltration making a favorable healing process.

### 3.4. SEM analysis

Fig. 10 represents the SEM micrograph of the interfacial region between the implant and the bone after 2 months post-operatively. The SEM photographs as shown by Fig. 10b have confirmed that the mineralization process for the Zn-doped HAp implant developed direct contact with the surrounding bone. In the sacrificed animals after 60 days of implantation, adequate roughness was evident on the surface of the both doped HAp implants and the bone tissues were found to grow into the finest irregularities. This study also revealed comparatively less bone in-growth and reduced mechanical anchorage to undoped HAp implant compared to doped HAp implants. Zone 1 showed the implant surface while zone 2 showed bone tissue. In pure HAp, even after 60 days gap (zone 3 in Fig. 10a) between implant and bone was clearly visible but in doped HAp, the whole interface was almost filled with newly formed bone tissue. Only some small gaps were found to still persist (zone 3 in Fig. 10b).

### 3.5. Oxytetracycline labeling study

Fig. 11 shows fluorochrome labeling images at 2 months post-surgery, exhibiting new bone formation as evidenced by golden yellow fluorescence where as sea green color appears host bone. In control, the activity of new bone formation was moderate. The micrograph for Zn-doped HAp showed more amount of new bone formation from both the ends as evidenced by golden yellow fluorescence. The osseous tissues originate both from periosteal and endosteal surface of bone; however, its intensity was more on endosteal side. The defect was entirely filled with newly formed bone and appeared as homogenous golden yellow area.

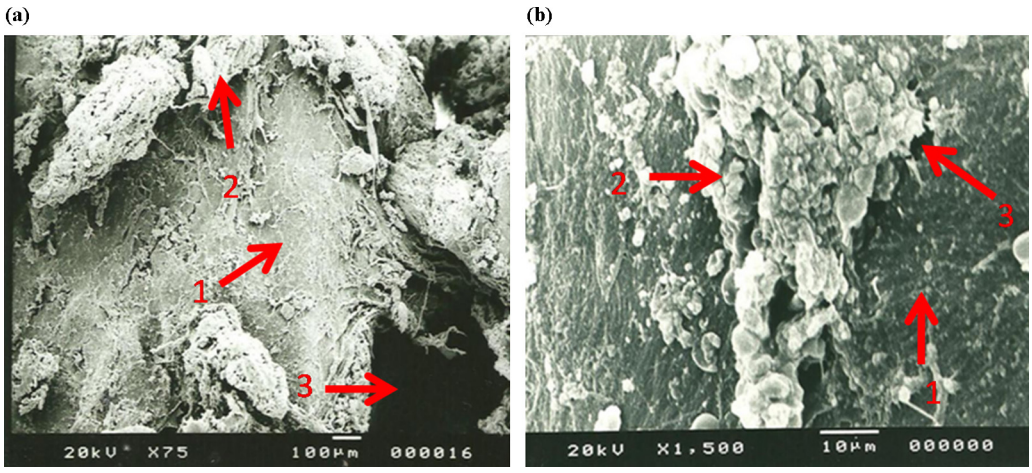


**Fig. 10.** SEM micrograph showing interfacial region between the HAp implant and surrounding hard tissue, a – pure HAp and b – doped HAp (1 – implant, 2 – new bone growth, 3 – gap between implant and host tissue).

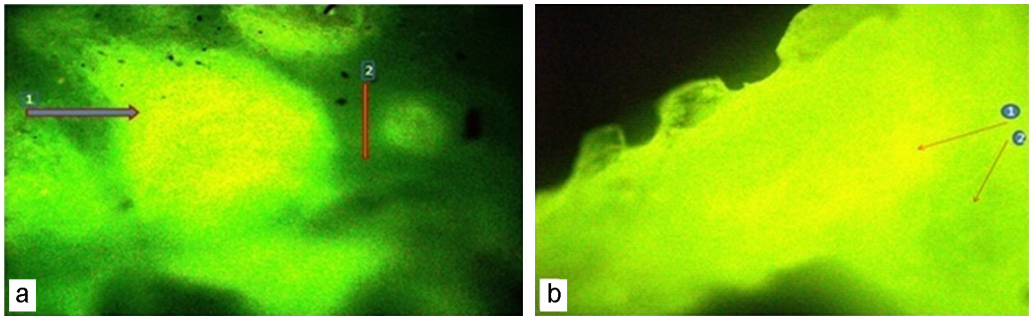


**Fig. 11.** Fluorochrome labeling images of (a) pure HAp and (b) doped HAp at 4 months post-operatively: new bone (arrow 1) and host bone (arrow 2).

### 3.6. Mechanical push-out testing

The interfacial bond strength of implanted pure and Zn-doped HAp was measured by mechanical push-out test after 2 months post operatively. Fig. 12a shows the average values of interfacial strength. The average interfacial strength of undoped HAp was found to be low ($2.38 \pm 0.47$ MPa). It was an average value from three such samples. The average value of interfacial strength for Zn-doped HAp implants was higher ($5.78 \pm 0.77$ MPa) compared with undoped HAp. This marked improvement may be attributed to more prominent tissue-implant interaction, which was evident from fluorochrome study and scanning electron microscopy. Fig. 12b shows a typical view of a doped HAp sample coming out from the bone during mechanical push-out test. Implant and the

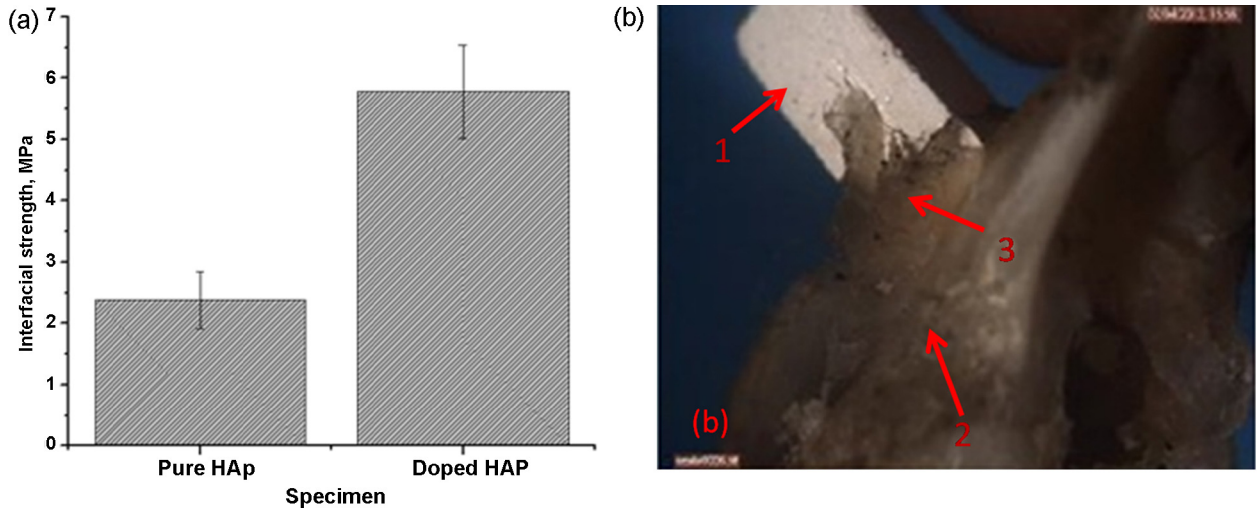


**Fig. 12.** (a) Interfacial strength of pure and doped HAp and (b) specimen coming out of the bone during mechanical push-out test (1 – specimen, 2 – surrounding tissue, 3 – interface region).

host tissues were shown by arrow by 1 and 2 respectively. The interfacial region shows clear signs of intense rubbing with some symptoms of wear and tear during ejection as shown by arrow 3. It indicated toward the presence of strong bonding between bone and implant.

From the above-mentioned observations, it may be summarized that in both the cases the microstructures revealed gross similarity, e.g., small, uniform, uni-axed grains with lot of interconnected pores. There was no significant difference from X-ray crystallography. But still Zn-doped HAp showed marked superiority in terms of new bone formation and bonding between bone and implant. Results of mechanical push-out test confirmed it in a quantitative manner. So the observed difference in in vivo performance can only be explained with the influence of Zn. Zn ion increases the activity of aminoacyl-tRNA synthetase, an enzyme which is involved in protein biosynthesis including the production of osteocalcin, IGF-1 and TGF-β in osteoblastic cells [18]. Zn has also role of targeting IGF binding proteins to the cell surface. It increases the activity of vitamin $D_3$-dependent promoters in osteoblasts [19]. Furthermore the presence of Zn ion triggers release of certain cytokines that have inhibitory effect on osteoclastic bone resorption. So at one hand, Zn promotes new bone formation by enhancing osteoblast activity and at the same time reduces bone resorption rate.

## 4. Conclusion

The results of the present study revealed that addition of Zn in HAp did not alter the major phase of the HAp. The crystallinity of Zn-doped HAp was not that high however the sintered density was nearly 85% with lot of interconnected pores. Zn ions partially replaced Ca ion and caused variation in the lattice structure, both in calcined powders and in sintered samples. The variation in lattice structure was found to be influenced by temperature due to temperature dependent evaporation of lattice $H_2O$. For doped specimens, (Ca + Zn)/P ratio was around 1.67, close to the stoichiometric Ca/P ratio in HAp. SBF study showed multilayered apatite formation on the surface of doped HAp specimens. Sequential radiological investigations showed progressively diminishing relative radio density of implant and surrounding host bone. SEM, histo-pathological study and oxytetracycline labeling study further confirmed superior bone–implant attachment of Zn-doped HAp. This was due to stimulatory effect of Zn ion on new bone formation and inhibitory effect to osteoclastic bone resorption.

## References

[1] J.F. Shackelford, Mater. Sci. Forum, 293, 1–4 (1999).
[2] T.S.B. Narasaraju and D.E. Phebe, J. Mater. Sci., 31, 1–21 (1996).
[3] F.S. Kaplan, W.C. Hayes, T.M. Keaveny, A. Boskey, T.A. Einhorn and J.P. Iannotti, American Association of Orthopaedic Surgeons (1994), pp. 127–184.
[4] A. Ito, H. Kawamura, M. Otsuka, M. Ikeuchi, H. Ohgushi, K. Ishikawa, K. Onuma, N. Kanzaki, Y. Sogo and N. Ichinose, Mater. Sci. Eng. C, 22, 21–25 (2002).
[5] A. Bigi, E. Foresti, M. Gandolfi, M. Gazzano and N. Roveri, J. Inorg. Biochem., 58, 49–58 (1995).
[6] T.J. Webster, C. Ergun, R.H. Doremus and R. Bizios, J. Biomed. Mater. Res., 59, 312–317 (2002).
[7] A. Bandyopadhyay, E.A. Withey, J. Moore and S. Bose, Mater. Sci. Eng. C, 27, 14–17 (2007).
[8] A. Ito, K. Ojima, H. Naito, N. Ichinose and T. Tateishi, J. Biomed. Mater. Res., 50, 178–183 (2000).
[9] X. Wang, A. Ito, Y. Sogo, X. Li and A. Oyane, Acta Biomater., 6, 962–968 (2010).
[10] Y. Li, Q. Li, S. Zhu, E. Lu, J. Li, G. Feng, Y. Liao and J. Hu, Biomaterials, 31, 9006–9014 (2010).
[11] T.J. Matsumoto, S.-H. An, T. Ishimoto, T. Nakano, T. Matsumoto and S. Imazato, Dent. Mater., 27, e205–e212 (2011).
[12] G. Lusvardi, D. Zaffe, L. Menabue, C. Bertoldi, G. Malavasi and U. Consolo, Acta Biomater., 5, 419–428 (2009).
[13] E. Landi, A. Tampieri, G. Celotti and S. Sprio, J. Eur. Ceram. Soc., 20, 2377–2387 (2000).
[14] B.D. Cullity, Elements of X-ray Diffraction, 2nd ed., Addison-Wesley, Reading, MA (1978).
[15] S. Koutsopoulos, J. Biomed. Mater. Res. A., 62, 600–612 (2002).
[16] F. Miyaji, Y. Kono and Y. Suyama, Mater. Res. Bull., 40, 209–220 (2005).
[17] S. Gomes, J.M. Nedelec and G. Renaudin, Acta Biomater., 8, 1180–1189 (2012).
[18] A. Ito, M. Otsuka, H. Kawamura, M. Ikeuchi, H. Ohgushi, Y. Sogo and N. Ichinose, Curr. Appl. Phys., 5, 402–406 (2005).
[19] W. Lutz, M.F. Burritt, D.E. Nixon, P.C. Kao and R. Kumar, Biochem. Biophys. Res. Commun., 271, (1) 1–7 (2000).